PAPER Special Section on Advanced Technologies in Antennas and Propagation in Conjunction with Main Topics of ISAP2009

Theoretical Estimation of Scattering Waves in Transverse Section of Upper Body for On-Body Wireless Communications

Changyong SEO[†a)], ***Student Member***, **Kazuyuki SAITO**[††], **Masaharu TAKAHASHI**[††], ***Members***, ***and*** **Koichi ITO**[†††], ***Fellow***

SUMMARY This paper attempts to analyze theoretically the propagation characteristics in the transverse section of upper body to support on-body wireless communications. The analytical estimation assumes that the human body is structured as a lossy-dielectric circular cylinder with infinite length that consists of the 2/3-muscle equivalent uniform tissue. Each scattering electric field formulation inside and outside of the cylinder is derived for scattering characteristics in the propagation environment including the human body when the source current has the vertical direction to the cylinder surface or the horizontal direction to the cylinder axis. In order to confirm the reliability of the formulation, total electric field distributions at 2.45 GHz are compared with the results by the finite-difference time-domain (FDTD) method. In each current direction, general scattering characteristics and the influence on the total propagation are estimated. Furthermore, from scattering and total electric field intensities evaluated with the variations of operating frequency, radius of the human body, and distance between a source and the human body, propagation characteristics are investigated to assist in the design of a device for on-body propagation channel with the upper body.

key words: *lossy-dielectric circular cylinder, on-body wireless communications, scattering waves*

1. Introduction

Over the last few decades, wireless-portable information and communication devices have begun to occupy a personal space in daily life. Such devices have been developed primarily as instruments for long-distance information-communications. In recent years, some novel wireless communication systems for applications leading to a more convenient and safer life have received great attention, and new technologies and general examinations in connection with the systems have been required [1], [2]. One of these is body-centric wireless communications which are classified as in-body, off-body, and on-body communication networks by the locations of the transmitter and receiver. The communication links for such networks are imaged in Fig. 1(a). For the design of a wearable or implant device operated in such networks, overriding considerations are respectively the surmounting of electrical properties of the human body, communication link between the human body and exterior environment, and propagation characteristics in the vicinity of the human body [3]–[5]. In cases of off-body and on-body communication channels, it is indispensable to consider the scattering waves including not only reflection and transmission but also specific physical propagations such as surface, leaky, and creeping waves in the inhomogeneous environment between the human body and the free space. For example, in a telemedicine application with biosensors which are distributed over the body surface to record the user's breathing, pulse, heartbeat, blood oxygen, etc., a wearable controller for data transmission between the biosensors and a remote station several meters away from the user is often included. In such application, both of on-body and off-body channels, which have the purposes of communications between the biosensors and the controller and between the controller and the station, respectively, are needed. In order to construct two channels, especially for on-body channel, the scattering waves generated in the vicinity of the human body may be utilized effectually. Thus, the overall estimation of propagation characteristics including scattering waves around the human body is significant for the design of a device. Nevertheless, few researches have been conducted on the propagation characteristics with the investigation of waves scattered by the human body. A wearable device, which aims to use the human body as a transmission channel, was analyzed by an equivalent circuit model, but the examination in relation to the influence of the human body was accomplished restrictively [6]. There was a study that evaluated the scattering waves theoretically with magnetic field solutions, but this evaluation was concentrated for the accuracy and validity of the high-frequency asymptotic analysis. The estimation of propagation characteristics from the relation between incident and scattering waves were not carried out [7]. Other explorations about propagation characteristics on the human body were confirmed principally with the FDTD method and experimental results [8], [9].

In this paper, in order to investigate analytically scattering characteristics for on-body wireless communications with the upper body as shown in Fig. 1(b), the formulations of scattering electric fields are first derived with the assumption that the upper body is a lossy-dielectric infinite uniform circular cylinder, and secondly the influence of scattering components on propagation characteristics is analyzed via the comparison between scattering and total field distributions. For more in-depth discussion, the evaluations with the variations of physical parameters such as operating fre-

Manuscript received January 4, 2010.
Manuscript revised May 7, 2010.

[†]The author is with the Graduate School of Science and Technology, Chiba University, Chiba-shi, 263-8522 Japan.
[††]The authors are with the Research Center for Frontier Medical Engineering, Chiba University, Chiba-shi, 263-8522 Japan.
[†††]The author is with the Graduate School of Engineering, Chiba University, Chiba-shi, 263-8522 Japan.
a) E-mail: ChangYong_SEO@graduate.chiba-u.jp

DOI: 10.1587/transcom.E93.B.2601

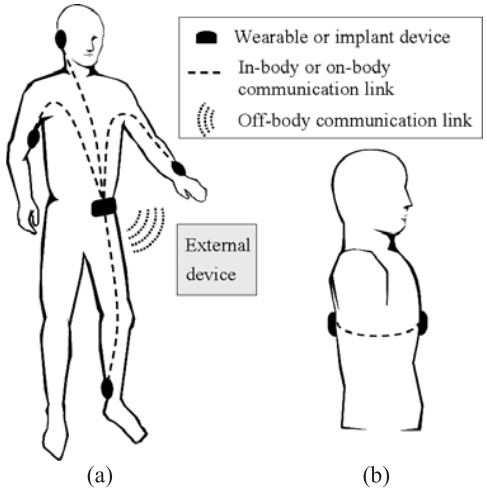

Fig. 1 (a) Communication links for body-centric wireless communications. (b) On-body communication link in transverse section of upper body as subject matter discussed in this paper.

quency, location of source, and radius of the human body are accomplished.

There are some differences between the assumption in this study and the environment with the real human body. For the theoretical analysis, therefore, it is above all premised on the comprehension in relation to the restrictions occurred from the differences. The first difference is that the real upper body consists of various tissues. However, because the kinds and sizes of tissues including the organs are different in accordance with an observation plane in the upper body, the detailed application of specific various tissues is impossible to obtain analytical solutions. For theoretical analysis, a multi-layered structure arranged with representative several tissues can approach to the real upper body, but nevertheless it is difficult to argue its appropriateness. For the same reason, many researches about body-centric wireless communications have been achieved with a representative uniform tissue being substituted for the real human body [6]–[8], and the theoretical analysis in this paper is performed also under the assumption that the upper body is a uniform tissue. The second difference is the finitude of length. The scattering waves in a finite-length structure comprise additionally the diffraction from the ends of finite structure. However, exact expressions for scattering waves in a finite-length model do not exist and the analytical solution can be approximately acquired only with a plane wave as the incident wave [10]. Main observation points in this paper are on the plane of circular transverse section as the same plane with a feeding point of source, and therefore the diffraction caused by finite length would be less influential on the whole levels of scattering waves than them at any other observation points. The third is the influence of multi-path propagating waves caused by other body parts except the upper body. In this paper, the waves are excluded because it can be expected that the amplitude of the waves is insignificant compared with the waves scattered by the upper body due to the absorption at other body parts and the attenuation about propagation distance. The fourth is that the transverse section of upper body is analogous to the shape of an ellipse even if the geometry for analysis is simplified. In the problem involving a dielectric elliptical cylinder, however, it is difficult to formulate with an orthogonal expansion for the Green's function since the angular and radial vector wave functions in an elliptical cylinder coordinate system depend on the wavenumber [11]. Accordingly, the structure of the circular cylinder, which has similar propagation characteristics, especially of scattering waves, in the environment with an elliptical cylinder-shaped scatterer, is adopted as the upper body in this paper.

Such differences between the real upper body and the geometry for analysis are sensitive with an operating frequency. In case of low frequencies which have larger wavelengths than the thickness or length of upper body, even if the tissue of the upper body is subdivided transversely, since the transverse sizes of split tissues in wavelength are very smaller than one wavelength, the scattering characteristics outer upper body would be little changed, compared with results from the use of uniform tissue. On the other hand, it is expected that the diffraction in connection with the finite-length of upper body and the multi-path propagation by other body parts have non-negligible effects at any observation point. Since the purpose of this paper is the evaluation of scattering waves involved in the overall geometrical feature related to the transverse section of upper body and general electrical characteristics of the human body, which are the high lossy-dielectric properties according to operating frequencies, the examinations concerned with frequency sweep in this paper are focused on comprehensive grasping of the frequency characteristics of general scattering waves excluding such diffraction and multi-path propagation at low frequencies.

This paper is constructed as follows. Section 2 describes the scattering electric field formulations inside and outside of the human body which is presumed to be a uniform tissue with the structure of infinite circular cylinder. The integral representations of eigenfunction solutions in cylindrical coordinates are derived when the current moment of source constitutes a vertical electric dipole (VED) to the cylinder surface and a horizontal electric dipole (HED) parallel to the cylinder axis. In Sect. 3.1, in order to certify the validity of the solutions, with VED and HED of a finite length and the 2/3-muscle equivalent tissue as the human body, the numerical results calculated with the analytical solutions explained in Sect. 2 are compared with the results obtained by the FDTD method. Furthermore, the general characteristics scattered by the human body and the influence on the total propagation are investigated. Section 3.2 presents results obtained from the variations of physical parameters which are concerned directly in scattering characteristics such as operating frequency, radius of the human body, and location of source. The propagation characteristics are evaluated to be useful for the practical design of a device for on-body wireless communications. Finally, Sect. 4

summarizes results and conclusions.

2. Scattering Electric Field Formulations

As the geometry for analysis, Fig. 2 shows the human body represented with a lossy-dielectric infinite circular cylinder of radius a in the free space. The human body has the electrical properties of conductivity σ and relative permittivity ε_r in accordance with operating frequency. The permittivity and permeability of the free space are ε_0 and μ_0, respectively. The angular frequency is designated as ω. The wavenumbers in regions 1 and 2 are k_1 and k_2, respectively. The types of current moment are representatively classified into VED and HED with $\boldsymbol{\rho}$- and $\boldsymbol{z}$-directions, respectively, as shown in Fig. 2.

The field emanated in region 1 can be identified by the method of scattering superposition and the field in region 2 is constructed only by scattering component as written in Eqs. (1) and (2). The notation $\boldsymbol{E}^{(ij)}$ is adopted when field point is in region i and source point is in region j. The superscripts 0 and S mean the incidence in the free space and the scattering by the cylinder, respectively.

$$\boldsymbol{E}^{(11)} = \boldsymbol{E}^{0} + \boldsymbol{E}^{\mathrm{S}(11)} \tag{1}$$

$$\boldsymbol{E}^{(21)} = \boldsymbol{E}^{\mathrm{S}(21)} \tag{2}$$

In cases of VED and HED with the current directions in Fig. 2, the incident electric field $\boldsymbol{E}^0$ can be easily achieved by the analysis of TM_x and TM_z modes, respectively, with the free-space Green's function of scalar wave equation [12]. The scattering problems having boundaries which coincide with cylindrical coordinate surfaces are firstly constructed from the solutions, which can be obtained by the method of separation of variables, satisfying the homogeneous scalar Helmholtz equation in cylindrical coordinate system. Linear combinations of the solutions are also solutions to the Helmholtz equation, and these can be expressed by the discrete summation over eigenvalue of constant n relative to only ϕ-domain and the integration over eigenvalue of k_z, which is the wavenumber of z-direction irrespective of regions in Fig. 2 [12], [13]. The eigenfunction for any values of such eigenvalues is solved explicitly by imposing boundary conditions at the interface $\rho = a$ between the cylinder and the free space [11], [14]. Through such a procedure for

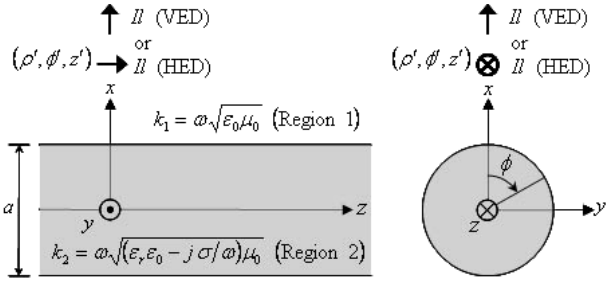

Fig. 2 Geometry for analysis. HED or VED with current moment Il is located at (ρ', ϕ', z') in region 1 of the free space. Region 2 with shading indicates the human body.

the eigenfunction solutions, when VED or HED with current moment Il is located at (ρ', ϕ', z'), scattering electric field formulations at observation point (ρ, ϕ, z) in region 1 are derived as written in Eqs. (3)–(5) or (6)–(8), respectively. In this paper, a time-harmonic convention of $e^{j\omega t}$ is assumed and suppressed.

$$E_{\rho}^{\mathrm{S}(11)\_\mathrm{V}} = -\frac{Il\omega\mu_0}{8\pi}\int_{-\infty}^{\infty}dk_z\sum_{n=0}^{\infty}\frac{(2-\delta_0)}{k_{\rho 1}^2}\cos\left(n\left(\phi-\phi'\right)\right)e^{-jk_z(z-z')}$$
$$\times\left[\left\{A_1\frac{n}{\rho}H_n^{(2)}\left(k_{\rho 1}\rho\right)+B_1\frac{jk_z}{k_1}\frac{\partial H_n^{(2)}\left(k_{\rho 1}\rho\right)}{\partial\rho}\right\}P\left(k_{\rho 1},n,k_z;\rho'\right)\right.$$
$$\left.+\left\{C_1\frac{jk_z}{k_1}\frac{\partial H_n^{(2)}\left(k_{\rho 1}\rho\right)}{\partial\rho}-D_1\frac{n}{\rho}H_n^{(2)}\left(k_{\rho 1}\rho\right)\right\}Q\left(k_{\rho 1},n,k_z;\rho'\right)\right] \tag{3}$$

$$E_{\phi}^{\mathrm{S}(11)\_\mathrm{V}} = -\frac{Il\omega\mu_0}{8\pi}\int_{-\infty}^{\infty}dk_z\sum_{n=0}^{\infty}\frac{(2-\delta_0)}{k_{\rho 1}^2}\sin\left(n\left(\phi-\phi'\right)\right)e^{-jk_z(z-z')}$$
$$\times\left[\left\{-A_1\frac{\partial H_n^{(2)}\left(k_{\rho 1}\rho\right)}{\partial\rho}-B_1\frac{jnk_z}{k_1\rho}H_n^{(2)}\left(k_{\rho 1}\rho\right)\right\}P\left(k_{\rho 1},n,k_z;\rho'\right)\right.$$
$$\left.+\left\{-C_1\frac{jnk_z}{k_1\rho}H_n^{(2)}\left(k_{\rho 1}\rho\right)+D_1\frac{\partial H_n^{(2)}\left(k_{\rho 1}\rho\right)}{\partial\rho}\right\}Q\left(k_{\rho 1},n,k_z;\rho'\right)\right] \tag{4}$$

$$E_{z}^{\mathrm{S}(11)\_\mathrm{V}} = -\frac{Il\omega\mu_0}{8\pi}\int_{-\infty}^{\infty}dk_z\sum_{n=0}^{\infty}\frac{(2-\delta_0)}{k_{\rho 1}^2}\cos\left(n\left(\phi-\phi'\right)\right)e^{-jk_z(z-z')}$$
$$\times\left[\left\{-B_1\frac{k_{\rho 1}^2}{k_1}H_n^{(2)}\left(k_{\rho 1}\rho\right)\right\}P\left(k_{\rho 1},n,k_z;\rho'\right)\right.$$
$$\left.+\left\{-C_1\frac{k_{\rho 1}^2}{k_1}H_n^{(2)}\left(k_{\rho 1}\rho\right)\right\}Q\left(k_{\rho 1},n,k_z;\rho'\right)\right] \tag{5}$$

$$E_{\rho}^{\mathrm{S}(11)\_\mathrm{H}} = -\frac{Il\omega\mu_0}{8\pi}\int_{-\infty}^{\infty}dk_z\sum_{n=0}^{\infty}\frac{(2-\delta_0)}{k_{\rho 1}^2}\cos\left(n\left(\phi-\phi'\right)\right)e^{-jk_z(z-z')}$$
$$\times\left[\left\{-C_1\frac{jk_z}{k_1}\frac{\partial H_n^{(2)}\left(k_{\rho 1}\rho\right)}{\partial\rho}+D_1\frac{n}{\rho}H_n^{(2)}\left(k_{\rho 1}\rho\right)\right\}R\left(k_{\rho 1},n,k_z;\rho'\right)\right] \tag{6}$$

$$E_{\phi}^{\mathrm{S}(11)\_\mathrm{H}} = -\frac{Il\omega\mu_0}{8\pi}\int_{-\infty}^{\infty}dk_z\sum_{n=0}^{\infty}\frac{(2-\delta_0)}{k_{\rho 1}^2}\sin\left(n\left(\phi-\phi'\right)\right)e^{-jk_z(z-z')}$$
$$\times\left[\left\{C_1\frac{jnk_z}{k_1\rho}H_n^{(2)}\left(k_{\rho 1}\rho\right)-D_1\frac{\partial H_n^{(2)}\left(k_{\rho 1}\rho\right)}{\partial\rho}\right\}R\left(k_{\rho 1},n,k_z;\rho'\right)\right] \tag{7}$$

$$E_{z}^{\mathrm{S}(11)\_\mathrm{H}} = -\frac{Il\omega\mu_0}{8\pi}\int_{-\infty}^{\infty}dk_z\sum_{n=0}^{\infty}\frac{(2-\delta_0)}{k_{\rho 1}^2}\cos\left(n\left(\phi-\phi'\right)\right)e^{-jk_z(z-z')}$$
$$\times\left[\left\{C_1\frac{k_{\rho 1}^2}{k_1}H_n^{(2)}\left(k_{\rho 1}\rho\right)\right\}R\left(k_{\rho 1},n,k_z;\rho'\right)\right] \tag{8}$$

where

$$P\left(k_{\rho 1}, n, k_z; \rho'\right) = \frac{n}{\rho'} H_n^{(2)}\left(k_{\rho 1}\rho'\right) \tag{9}$$

$$Q\left(k_{\rho 1}, n, k_z; \rho'\right) = -\frac{jk_z}{k_1}\frac{\partial H_n^{(2)}\left(k_{\rho 1}\rho'\right)}{\partial \rho} \tag{10}$$

$$R\left(k_{\rho 1}, n, k_z; \rho'\right) = \frac{k_{\rho 1}^2}{k_1} H_n^{(2)}\left(k_{\rho 1}\rho'\right) \tag{11}$$

δ_0 is the Kronecker delta function, which is 1 if $n = 0$, and 0 otherwise. $k_{\rho 1} = -\sqrt{k_1^2 - k_z^2}$ and $H_n^{(2)}(x)$ is the Hankel function of the second kind of order n. The coefficients A_1, B_1, C_1, and D_1 deduced from boundary conditions are explained in the Appendix. The expressions in square brackets in Eqs. (3)–(8) are organized individually with the functions corresponding to observation point and the functions of source points as written in Eqs. (9)–(11).

Field formulations of $\boldsymbol{E}^{\mathrm{S}(21)}$ for observation point inner cylinder is attained basically by altering the variables associated with region 1 in braces in Eqs. (3)–(8) into the variables in region 2. Furthermore, the Bessel function should be substituted for the Hankel function because the radiation condition at the origin where $\rho = 0$ has to be satisfied. Namely, the variables A_1, B_1, C_1, D_1, k_1, $k_{\rho 1}$, and the function $H_n^{(2)}\left(k_{\rho 1}\rho\right)$ in braces are changed into a_2, b_2, c_2, d_2, k_2, $k_{\rho 2}$, and $J_n\left(k_{\rho 2}\rho\right)$, respectively. $k_{\rho 2} = -\sqrt{k_2^2 - k_z^2}$, $J_n(x)$ is the Bessel function of the first kind of order n, and the coefficients a_2, b_2, c_2, and d_2 from boundary conditions in relation to region 2 are also described in the Appendix.

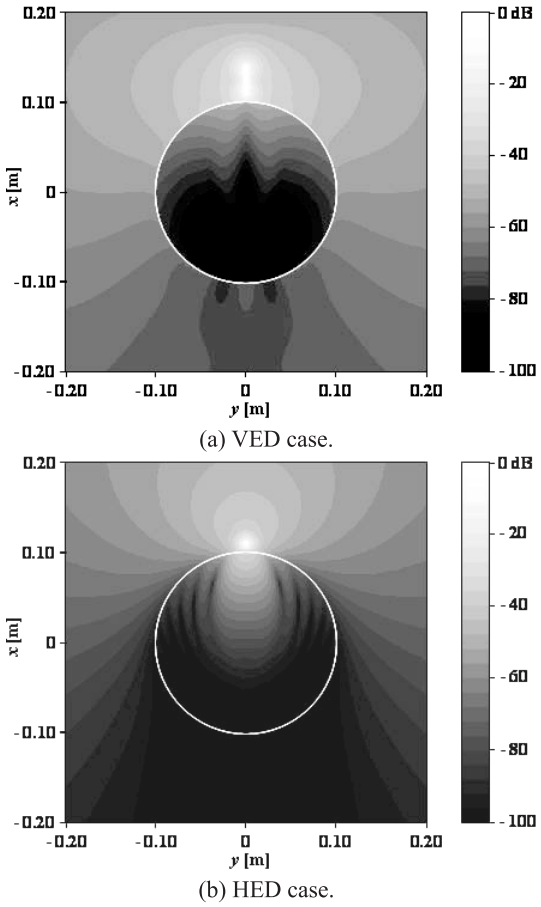

(a) VED case.

(b) HED case.

Fig. 3 Total electric field distributions calculated by the FDTD method.

3. Numerical Results and Discussion

3.1 Electric Field Distributions in Transverse Section

In this section, in order to verify the reliability of the scattering electric field formulations derived in Sect. 2, the comparison between the results calculated by the FDTD method and with the analytical solutions is performed at 2.45 GHz in the industrial, scientific, and medical (ISM) radio bands. The radius a of cylinder represented as the upper body is set as 0.10 m which is near the average of median chest width of the Japanese [15]. The inner cylinder assumed to be a homogeneous single tissue has electrical properties of the 2/3-muscle equivalent tissue, $\sigma = 1.16$ S/m, $\varepsilon_r = 35.15$ at 2.45 GHz [16]. A linear dipole which has the structure of VED or HED with 0.03 m length is employed, and the source is located at 0.01 m away from the cylinder surface. With the coordinate system in Fig. 2, feeding points (x', y', z') of VED and HED placed at the center of linear dipole are at (0.1025 m, 0, 0) and (0.1100 m, 0, 0), respectively. The observation plane is xy-plane at $z = 0$.

In the calculation with the FDTD method, the cell size is $\Delta x = \Delta y = \Delta z = 2$ mm and the perfect matching layer (PML) of eight layers is used as the absorbing boundary condition. The cylinder is extended into inner PML for materialization of the infinite cylinder. In the radiation problem solved with the analytical solutions, the integral over the wavenumber k_z is worked out by applying the Gauss-Legendre integration excluding intentionally the singularities of $k_z = \pm k_1$.

In cases of VED and HED, the calculation results by the FDTD method are exhibited in Figs. 3(a) and (b), respectively. With the same cases, Figs. 4 and 5, respectively, are the numerical results evaluated with the analytical solutions. Each (a) and (b) in Figs. 4 and 5 are the distributions of total electric fields and scattering electric fields, respectively. All results in Figs. 3–5 are displayed with the relative values normalized by the total electric fields at the nearest cell-points of y-direction from the feeding points. The standard level 0 dB in the results with VED and HED means the absolute values of total electric fields at (x, y, z) = (0.1025 m, 0.0020 m, 0) and (0.1100 m, 0.0020 m, 0), respectively. The white circle line in Figs. 3–5 indicates the interface between the cylinder and the free space.

The results by the FDTD method and with the eigenfunction solutions are in near-perfect agreement except that a slight difference is observed only when a source is the VED type and the observation point is near $\phi - \phi' = 180$ degrees outside the cylinder. That is an error in the FDTD method which cannot take shape the calculation model of a perfect circular transverse section. From the results with VED source as shown in Fig. 4, the field distribution inner

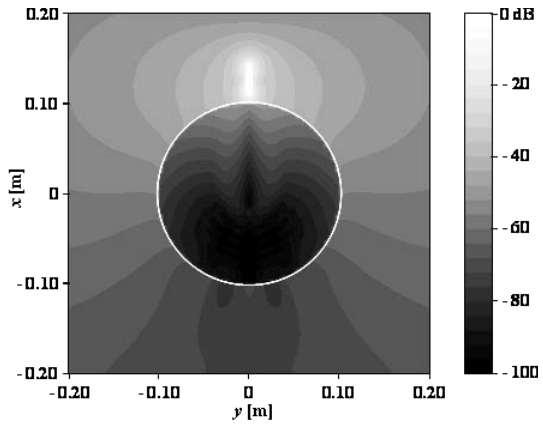

(a) Total electric field distribution.

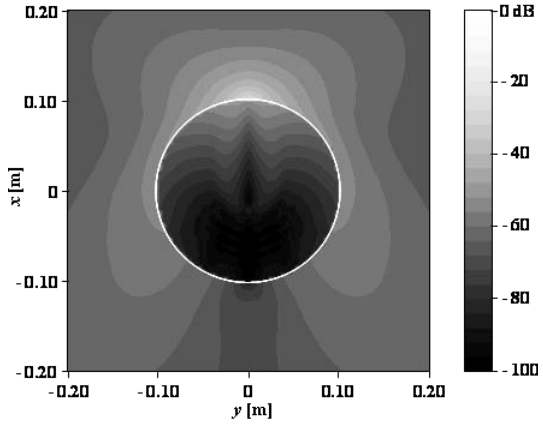

(b) Scattering electric field distribution.

Fig. 4 Electric field distributions of VED case calculated with the eigenfunction solutions.

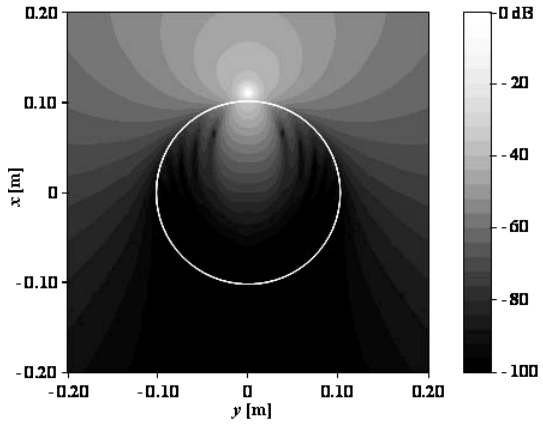

(a) Total electric field distribution.

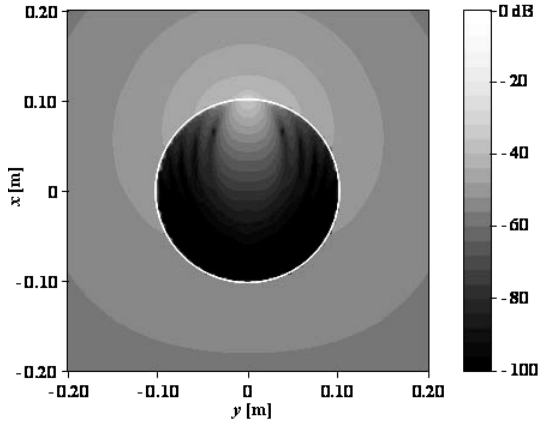

(b) Scattering electric field distribution.

Fig. 5 Electric field distributions of HED case calculated with the eigenfunction solutions.

cylinder is guided in ϕ-domain and the field intensities are attenuated abruptly due to the high conductivity. The scattering waves of the outward cylinder evaluated in Fig. 4(b) have the distribution enclosing the cylinder. The existence of a creeping wave mode is ascertained at the interface between the cylinder and the free space. As the general view about scattering waves, especially in relation with the reflected waves which is a representative component of scattering waves, the intensities of scattering waves are usually lower than levels of incident waves because scattering waves involves the exponential decline according to the propagation distance to a scatterer. Therefore, the total field distribution shown in Fig. 4(a) is, on the whole, similar to the incident field distribution of a VED although the scattering waves may be distributed influentially such as Fig. 4(b). In Fig. 4(a), however, the total fields near the cylinder surface and at the opposite side of cylinder are distributed as the shape deviated from the general incident-field distribution. By the comparison with the scattering field distribution displayed in Fig. 4(b), at such areas, it can be confirmed that the scattering waves with higher level than the incident waves affect immediately on the total field distribution. The greatest influence of the scattering waves including creeping waves is expected at $\phi - \phi' = 180$ degrees where the observation point has the weakest incidence, but the field distribution with relatively high intensities is not observed on account of the high conductivity-loss inner cylinder and the propagation loss in connection with the large cylinder radius. As discussions in case of HED source, firstly, the scattering fields in the free space as manifested in Fig. 5(b) have the isotropic distribution similarly to incident field distribution. As the cylinder axis and source direction are identical as z-direction and the analysis has the homogeneous environment in regard to that direction, the isotropic scattering waves are distributed in xy observation-plane. The center point of the isotropic scattering waves is the closest cylinder surface to the source, and this can be considered as the simple reflection phenomenon by the cylinder. As the distance between the source and cylinder is very small compared to the wavelength in the free space, there is little difference between the isotropic distributions of incident and scattering electric fields and therefore the incidence is generally counterbalanced by the scattering components. In particular, the total electric field distribution at the opposite side of cylinder, where the incident and scattering intensities are low, has the extremely low levels as shown in Fig. 5(a). The attenuation of the field inner cylinder is observed along x-direction as the main propagation direction. From Fig. 5 and its dis-

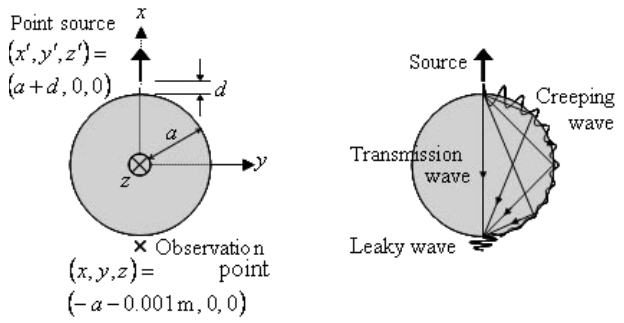

(a) Calculation setup. (b) Propagation modes.

Fig. 6 Coordinates of source and observation point, and physical picture of multi-path propagations.

cussions, it is corroborated that current moments of HED type contribute little for on-body wireless communications which make the propagation channel on the opposite side of the human body.

3.2 Electric Fields with Variations of Physical Parameters

When a specific scatterer is implicated in the environment for analysis, the total propagation is determined by incident and scattering waves. Therefore, only one of the waves cannot represent total characteristics, and the analysis of the interrelation between two waves is necessary. In Fig. 2 for theoretical analysis of on-body wireless communications, the parameters affecting scattering waves are cylinder radius, distance between source and cylinder surface, and operating frequency. Due to the fact that electrical properties of the human body vary with frequency, the operating frequency is a very important consideration in body-centric wireless communications [16]. The standard value at a fixed observation point is necessary for the relative level. However, when the frequency sweep is examined, the result usually cannot be normalized with the value at a fixed point owing to the variation of electrical distance from a source to the point. All values of results in this section are expressed with dBV/m, which the absolute electric field unit V/m is converted on a logarithmic scale in decibels for explicit display.

With the cylinder having electrical features of the 2/3-muscle equivalent tissue in accordance with operating frequency, Figs. 7 and 8 show absolute values of electric field with the variations of parameter d designated in Fig. 6(a) and operating frequency. As the results with the parameter $a = \pm\ 0.01 + 0.10$ m, which is considered the tolerance of median chest width by different persons, the observation point is the closest point to the surface on the opposite side of cylinder, that is $(x, y, z) = (-a - 0.001\,\mathrm{m}, 0, 0)$ as shown in Fig. 6(a). A source employed in this section is the VED-type point source located at $(x', y', z') = (a + d, 0, 0)$ with the current of 0.02 A. The reason a point source is used is to be helpful for the design of a device, e.g. the effective length of device or the location of feeding point, through the exact evaluation in relation to parameter d. As the calculation is accomplished with $\phi - \phi' = 180$ degrees and $z - z' = 0$, the ρ

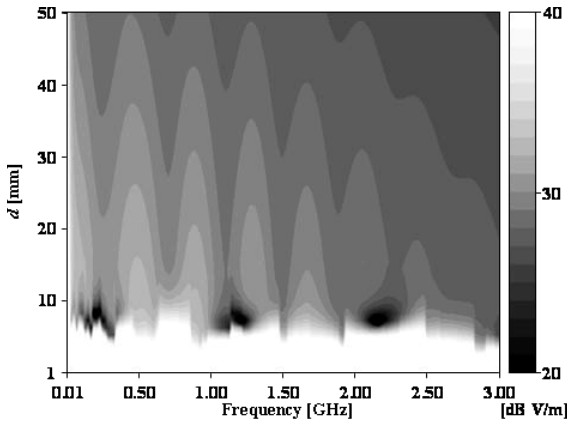

(a) Total electric fields.

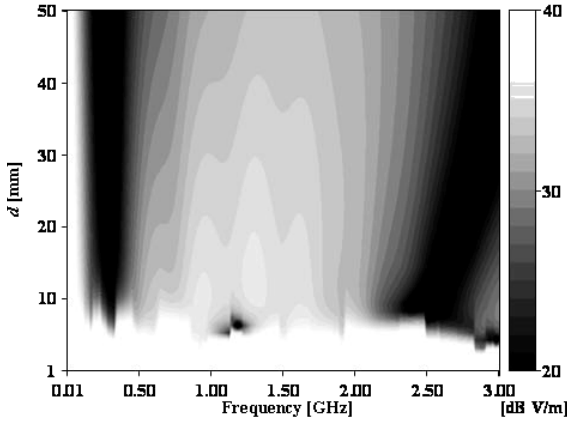

(b) Scattering electric fields.

Fig. 7 Electric field intensities with variations of parameter d and operating frequency when $a = 0.09$ m.

component of electric field only exists. In Figs. 7 and 8, each (a) shows the total electric fields and each (b) demonstrates the results of scattering components.

As shown in Fig. 6(b), the scattering waves are evaluated synthetically through multi-path propagations. By the propagation paths, the scattering waves at the shadowed space of cylinder are categorized typically into the transmission wave with the straight path between source and observation point, the leaky waves from the guided waves inner cylinder mentioned in Sect. 3.1, and the creeping waves generated along the cylinder surface.

Both scattering results shown in Figs. 7(b) and 8 (b) have null lines at some specific frequency bands. These null lines are caused by countervailing among the scattering components with different propagation paths. The phase-offset can be explained when the electrical lengths of the paths are changed due to the variation of wavelength. In the same vein, the null lines in Fig. 8(b) of $a = 0.11$ m appear in the lower frequency band than the null lines in Fig. 7(b) of $a = 0.09$ m due to the variation of the electrical path length by increasing the cylinder radius. It can be predicted that the null lines in scattering results would appear to be tilting steeply toward the axis of parameter d in periodic frequency band if the calculation is performed at a higher and wider

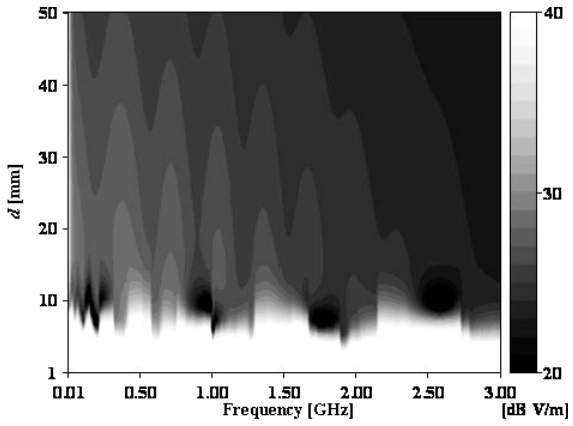

(a) Total electric fields.

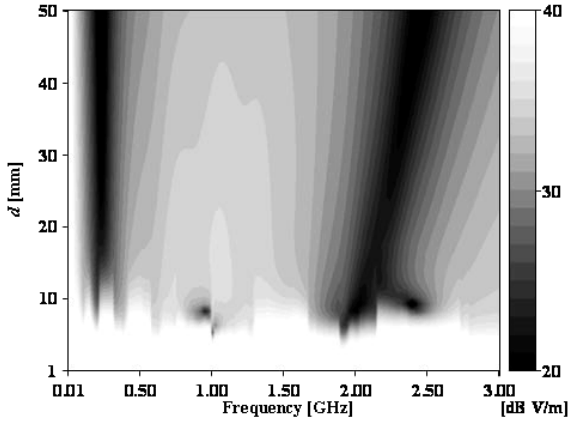

(b) Scattering electric fields.

Fig. 8 Electric field intensities with variations of parameter d and operating frequency when a = 0.11 m.

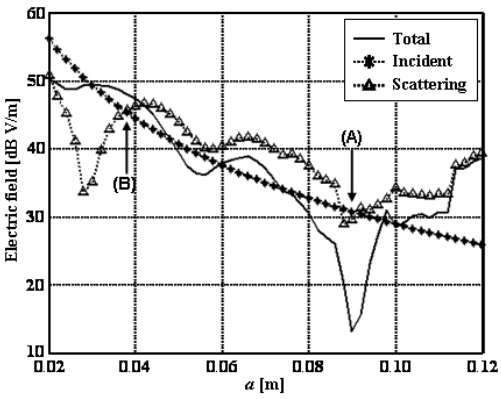

(a) At 1.21 GHz and d = 8 mm.

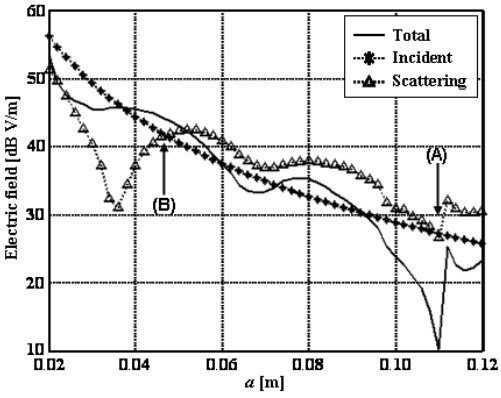

(b) At 0.97 GHz and d = 10 mm.

Fig. 9 Electric field intensities with variation of cylinder radius a when operating frequency and parameter d are fixed.

operating frequency range. The conductivity inner cylinder with electrical properties of the 2/3-muscle equivalent tissue increases in proportion to operating frequency [16]. Although a large conductive loss at a high operating frequency can be guessed, the attenuation relative to the conductivity is not visible in the scattering results. Thus, in relation to the variation of operating frequency, it can be estimated that the scattering waves have been affected by the electrical length of propagation path than the conductive loss. When the parameter d is less than 6 mm in Fig. 7(b) and 8 mm in Fig. 8(b), the scattering levels are extremely high in all frequency ranges calculated and no null line appears. This phenomenon is basically due to the fact that initial level transmitted to the cylinder is high. As shown Fig. 6(b), the leaky waves generated from guided modes focused at the cylinder surface near the observation point have various propagation paths, whereas the transmission wave has only a direct propagation path. Even if the conductive loss inner cylinder in the guided modes is considered, the contribution of the leaky waves cannot be neglected. The creeping waves are not unrestricted either from the conductive loss inner cylinder, but a creeping wave mode associated with low attenuation by the high conductivity may exist, such as the creeping wave mode on a dielectric coated conducting cylinder [17].

Notable is that such high levels of the scattering waves is preserved in the total electric field results shown in Figs. 7(a) and 8 (a). This result indicates that the device structure with current moment of VED type and thickness less than 6 mm from the surface of the human body is advantageous to make the propagation channel for on-body wireless communications using the upper body. The levels in Fig. 8(a) by and large are lower than the levels in Fig. 7(a) because the observation point becomes more distant from the source due to the increase of the cylinder radius. When a source is located at a certain height above the cylinder, the total electric field intensities are lower on account of the offset between incident and scattering waves as shown in Figs. 7(a) and 8 (a). For the same reason mentioned in the discussion for scattering waves, such counterbalance takes the shape of periodic distribution in the axis of frequency and several null points are observed at certain points with particular frequency and parameter d.

In reference to the null points appeared at 1.21 GHz in Fig. 7(a) and 0.97 GHz in Fig. 8(a), Fig. 9 describes the results of incident, scattering, and total waves with the variation of cylinder radius a. The total electric field intensity drops precipitously at a = 0.09 m and a = 0.11 m of points (A) in Figs. 9(a) and (b), respectively. The incident and scattering levels at the points are almost same and therefore

it can be deduced that the two waves counterbalance each other. However, at other points with almost identical intensities between incident and scattering electric fields, those are $a = 0.38$ m and $a = 0.46$ m designated by points (B), respectively, in Figs. 9(a) and (b), the two waves complement each other. This explains why the null points in Figs. 7(a) and 8(a) become visible from the offset, restricted with the calculation conditions of $a = 0.09$ m and $a = 0.11$ m. However, there is a need to be cautious with regard to such null points in the design of a device for on-body communication channel aimed in the transverse section of upper body.

4. Conclusions

In this paper, in order to estimate the propagation characteristics for on-body wireless communications using the upper body, the scattering waves by the human body have been calculated and the contribution of them to the total propagation has been investigated. For theoretical estimation, the structure of the human body was simplified as a lossy-dielectric infinite circular cylinder, and the 2/3-muscle equivalent uniform tissue are substituted for the inner human body. Firstly, in cases of VED and HED, each scattering electric field formulations were derived as the integral representations of the eigenfunction solutions in cylindrical coordinates. The exactitude of the formulations was verified by the comparison with the results calculated by the FDTD method.

From the scattering and total electric field distributions in the transverse section of the cylinder, the general characteristics scattered by the human body were investigated and it was confirmed that to make the propagation channel at the shadowed space was difficult with only a HED-type source.

The estimations with the variations of operating frequency, radius of the human body, and location of source were accomplished. From the results, the characteristics of scattering waves, which are classified largely as transmission wave, leaky waves, and creeping waves, were analyzed when the human body became a scatterer. With the results, it was shown that the VED-type source with the current distribution below 6 mm from the surface of the human body was able to build up the propagation channel composed mainly by the scattering components for on-body wireless communications aimed in the transverse section of upper body. Furthermore, it was explained that the worst cases in connection with the propagation at the opposite side of the human body existed restrictively at certain specific operating frequencies and locations of source.

In reference to this paper, in order to better comprehend the scattering waves created by the human body, an analysis about scattering components in body-centric wireless communications will be attempted as the next step.

References

[1] M. Weiser, "The computer for the twenty-first century," Scientific American, pp.66–75, Sept. 1991.
[2] T.G. Zimmerman, "Personal area networks: Near-field intra-body communication," IBM Syst. J., vol.35, no.3, pp.609–617, 1996.
[3] B.M. Steinhaus, R.E. Smith, and P. Crosby, "The role of telecommunications in future implantable device systems," Proc. IEEE Conference on Medicine and Biology, pp.1013–1014, Nov. 1994.
[4] N. Haga, K. Saito, M. Takahashi, and K. Ito, "Characteristics of cavity slot antenna for body-area networks," IEEE Trans. Antennas Propag., vol.57, no.4, pp.837–843, April 2009.
[5] P.S. Hall and Y. Hao, Antennas and Propagation for Body-Centric Wireless Communications, Artech House, Norwood, MA, 2006.
[6] K. Fujii, M. Takahashi, and K. Ito, "Electric field distributions of wearable devices using the human body as a transmission channel," IEEE Trans. Antennas Propag., vol.55, no.7, pp.2080–2087, July 2007.
[7] T. Sasamori, M. Takahashi, and T. Uno, "Transmission mechanism of wearable device for on-body wireless communications," IEEE Trans. Antennas Propag., vol.57, no.4, pp.936–942, April 2009.
[8] G.A. Conway and W.G. Scanlon, "Antennas for over-body-surface communications at 2.45 GHz," IEEE Trans. Antennas Propag., vol.57, no.4, pp.844–855, April 2009.
[9] R. Mittra, J. Bringuier, and J. Wiart, "Modeling of propagation on and interaction between body-mounted antennas," Proc. 2007 IET Seminar on Antennas and Propagation for Body-Centric Wireless Communications, p.5, April 2007.
[10] P.D. Matthaeis and R.H. Lang, "Comparison of surface and volume currents models for electromagnetic scattering from finite dielectric cylinders," IEEE Trans. Antennas Propag., vol.57, no.7, pp.2216–2220, July 2009.
[11] C.T. Tai, Dyadic green functions in electromagnetic fields, 2nd ed., IEEE, New York, 1993.
[12] R.F. Harrington, Time-harmonic electromagnetic fields, IEEE, New York, 2001.
[13] W.C. Chew, Waves and fields in inhomogeneous media, IEEE, New York, 1995.
[14] L.B. Felsen and N. Marcuvitz, Radiation and scattering of waves, IEEE, New York, 1994.
[15] Human body dimensions data for ergonomic design, Report of national institute of bioscience and human-technology, vol.2, no.1, pp.83–84, 1994.
[16] S. Gabriel, R.W. Lau, and C. Gabriel, "The dielectric properties of biological tissues: II. Measurements in the frequency range 10 Hz to 20 GHz," Physics in Medicine and Biology, vol.41, pp.2251–2269, 1996.
[17] R. Paknys and D.R. Jackson, "The relation between creeping waves, leaky waves, and surface waves," IEEE Trans. Antennas Propag., vol.53, no.3, pp.898–907, March 2005.

Appendix

Scattering Coefficients

For the construction of scattering field formulations associated with an infinite cylinder, it is necessary firstly to expand the eigenfunction of the Green's function in the free space. In accordance with the kind of cylinder, scattering coefficients are attached to the expanded eigenfunction solutions. By the method to satisfy boundary conditions at the interface ($\rho = a$) between the cylinder and the external environment, the coefficients are determined with the forms of simultaneous equations. In the case of a lossy-dielectric cylinder conducted in this paper, the scattering coefficients are arranged as follows:

$$A_1 = -\frac{J_n\left(k_{\rho 1}a\right)}{H_n^{(2)}\left(k_{\rho 1}a\right)}$$

$$-\frac{j2}{\pi\left(k_{\rho1}a\right)}\frac{T_n\left(k_{\rho1},k_{\rho2};a\right)}{\left[\left(k_{\rho1}a\right)H_n^{(2)}\left(k_{\rho1}a\right)\right]^2 U_n\left(k_{\rho1},k_{\rho2};a\right)} \quad (A\cdot 1)$$

$$B_1=\frac{2}{\pi\left(k_{\rho1}a\right)}\frac{W\left(k_{\rho1},k_{\rho2};a\right)}{a\left[\left(k_{\rho1}a\right)H_n^{(2)}\left(k_{\rho1}a\right)\right]^2 U_n\left(k_{\rho1},k_{\rho2};a\right)}\left(\frac{nk_z}{k_1}\right) \quad (A\cdot 2)$$

$$C_1=-\frac{J_n\left(k_{\rho1}a\right)}{H_n^{(2)}\left(k_{\rho1}a\right)} -\frac{j2}{\pi\left(k_{\rho1}a\right)}\frac{S_n\left(k_{\rho1},k_{\rho2};a\right)}{\left[\left(k_{\rho1}a\right)H_n^{(2)}\left(k_{\rho1}a\right)\right]^2 U_n\left(k_{\rho1},k_{\rho2};a\right)} \quad (A\cdot 3)$$

$$D_1=B_1 \quad (A\cdot 4)$$

$$a_2=-\frac{j2}{\pi\left(k_{\rho1}a\right)}\frac{\mu T_n\left(k_{\rho1},k_{\rho2};a\right)}{\left(k_{\rho2}a\right)^2 J_n\left(k_{\rho2}a\right)H_n^{(2)}\left(k_{\rho2}a\right)U_n\left(k_{\rho1},k_{\rho2};a\right)} \quad (A\cdot 5)$$

$$b_2=\frac{2}{\pi\left(k_{\rho1}a\right)}\frac{\sqrt{\mu\varepsilon}W\left(k_{\rho1},k_{\rho2};a\right)}{a\left(k_{\rho2}a\right)^2 J_n\left(k_{\rho2}a\right)H_n^{(2)}\left(k_{\rho2}a\right)U_n\left(k_{\rho1},k_{\rho2};a\right)}\left(\frac{nk_z}{k_1}\right) \quad (A\cdot 6)$$

$$c_2=-\frac{j2}{\pi\left(k_{\rho1}a\right)}\frac{\sqrt{\mu\varepsilon}S_n\left(k_{\rho1},k_{\rho2};a\right)}{\left(k_{\rho2}a\right)^2 J_n\left(k_{\rho2}a\right)H_n^{(2)}\left(k_{\rho2}a\right)U_n\left(k_{\rho1},k_{\rho2};a\right)} \quad (A\cdot 7)$$

$$d_2=\sqrt{\mu/\varepsilon}b_2 \quad (A\cdot 8)$$

$$U_n\left(k_{\rho1},k_{\rho2};a\right)=S_n\left(k_{\rho1},k_{\rho2};a\right)T_n\left(k_{\rho1},k_{\rho2};a\right) -\left(\frac{nk_z}{k_1a}\right)^2\left(W\left(k_{\rho1},k_{\rho2};a\right)\right)^2 \quad (A\cdot 9)$$

$$S_n\left(k_{\rho1},k_{\rho2};a\right)=\frac{\partial H_n^{(2)}\left(k_{\rho1}a\right)/\partial a}{\left(k_{\rho1}a\right)^2 H_n^{(2)}\left(k_{\rho1}a\right)}-\mu\frac{\partial J_n\left(k_{\rho2}a\right)/\partial a}{\left(k_{\rho2}a\right)^2 J_n\left(k_{\rho2}a\right)} \quad (A\cdot 10)$$

$$T_n\left(k_{\rho1},k_{\rho2};a\right)=\frac{\partial H_n^{(2)}\left(k_{\rho1}a\right)\big/\partial a}{\left(k_{\rho1}a\right)^2 H_n^{(2)}\left(k_{\rho1}a\right)}-\varepsilon\frac{\partial J_n\left(k_{\rho2}a\right)\big/\partial a}{\left(k_{\rho2}a\right)^2 J_n\left(k_{\rho2}a\right)} \quad (A\cdot 11)$$

$$W\left(k_{\rho1},k_{\rho2};a\right)=\frac{1}{\left(k_{\rho1}a\right)^2}-\frac{1}{\left(k_{\rho2}a\right)^2} \quad (A\cdot 12)$$

where $\varepsilon=(\varepsilon_r\varepsilon_0-j\sigma/\omega)/\varepsilon_0$ and $\mu=\mu_0/\mu_0=1$ are the ratios of permittivity and permeability, respectively, between regions 1 and 2 in Fig. 2.

Changyong Seo was born in Korea, on July 1976. He received the B.E. and M.E. degrees from Chungnam Nat. University, Daejeon, Korea, in 2003 and 2005, respectively. He is presently with the Graduate School of Science and Technology, Chiba University, Japan where he is working toward the Ph.D. degree. His main interest is the theoretical analysis and practical design for small antennas and body-centric wireless communication devices. Mr. Seo received the International Symposium on Antennas and Propagation (ISAP) Student Paper Contest Prize and Poster Presentation Award in 2007.

Kazuyuki Saito was born in Nagano, Japan, in May 1973. He received the B.E., M.E. and D.E. degrees all in electronic engineering from Chiba University, Chiba, Japan, in 1996, 1998, and 2001, respectively. He is currently an Assistant Professor with the Research Center for Frontier Medical Engineering, Chiba University. His main interest is in the area of medical applications of the microwaves including the microwave hyperthermia. Dr. Saito received the IEICE AP-S Freshman Award, the Award for Young Scientist of URSI General Assembly, the IEEE AP-S Japan Chapter Young Engineer Award, the Young Researchers' Award of IEICE, and the International Symposium on Antennas and Propagation (ISAP) Paper Award in 1997, 1999, 2000, 2004, and 2005 respectively. He is a member of the Institute of Electrical and Electronics Engineers (IEEE), the Institute of Image Information and Television Engineers (ITE), Japan, and the Japanese Society for Thermal Medicine.

Masaharu Takahashi was born in Chiba, Japan, on December, 1965. He received the B.E. degree in electrical engineering in 1989 from Tohoku University, Miyagi, Japan, and the M.E. and D.E. degrees both in electrical engineering from Tokyo Institute of Technology, Tokyo, Japan, in 1991 and 1994 respectively. He was a Research Associate from 1994 to 1996, and an Assistant Professor from 1996 to 2000 at Musashi Institute of Technology, Tokyo, Japan. He was an Associate Professor from 2000 to 2004 at Tokyo University of Agriculture and Technology, Tokyo, Japan. He is currently an Associate Professor at the Research Center for Frontier Medical Engineering, Chiba University. His main interests are electrically small antennas, planar array antennas, and electromagnetic compatibility. Dr. Takahashi is a member of the Institute of Electrical and Electronics Engineers (IEEE). He received the IEEE Antennas and Propagation Society (IEEE AP-S) Tokyo chapter Young Engineer Award in 1994.

Koichi Ito was born in Nagoya, Japan, in June 1950. He received the B.S. and M.S. degrees from Chiba University, Chiba, Japan, in 1974 and 1976, respectively, and the D.E. degree from Tokyo Institute of Technology, Tokyo, Japan, in 1985, all in electrical engineering. From 1976 to 1979, he was a Research Associate at the Tokyo Institute of Technology. From 1979 to 1989, he was a Research Associate at Chiba University. From 1989 to 1997, he was an Associate Professor at the Department of Electrical and Electronics Engineering, Chiba University, and is currently a Professor at the Graduate School of Engineering, Chiba University. From 2005 to 2009, he was Deputy Vice-President for Research, Chiba University. From 2008 to 2009, he was Vice-Dean of the Graduate School of Engineering, Chiba University. Since April 2009, he has been appointed as Director of Research Center for Frontier Medical Engineering, Chiba University. In 1989, 1994, and 1998, he visited the University of Rennes I, France, as an Invited Professor. His main research interests include analysis and design of printed antennas and small antennas for mobile communications, research on evaluation of the interaction between electromagnetic fields and the human body by use of numerical and experimental phantoms, microwave antennas for medical applications such as cancer treatment, and antenna systems for body-centric wireless communications. Professor Ito is a Fellow of the IEEE, and a member of AAAS, the Institute of Image Information and Television Engineers of Japan (ITE) and the Japanese Society for Thermal Medicine. He served as Chair of the Technical Group on Radio and Optical Transmissions, ITE from 1997 to 2001, Chair of the Technical Committee on Human Phantoms for Electromagnetics, IEICE from 1998 to 2006, Chair of the IEEE AP-S Japan Chapter from 2001 to 2002, TPC Co-Chair of the 2006 IEEE International Workshop on Antenna Technology (iWAT2006), Vice-Chair of the 2007 International Symposium on Antennas and Propagation (ISAP2007) in Japan, General Chair of iWAT2008, Co-Chair of ISAP2008 and an AdCom member for the IEEE AP-S from 2007 to 2009. He currently serves as an Associate Editor for the *IEEE Transactions on Antennas and Propagation*, a Distinguished Lecturer for the IEEE AP-S, and Chair of the Technical Committee on Antennas and Propagation, IEICE. He has been appointed as General Chair of ISAP2012 to be held in Nagoya, Japan in 2012.